Glucose-Sensitive Inverse Opal Hydrogels: Analysis of Optical Diffraction Response

Yun-Ju Lee, Stephanie A. Pruzinsky, and Paul V. Braun*

Department of Materials Science and Engineering, Beckman Institute for Advanced Science and Technology, and Frederick Seitz Materials Research Laboratory, University of Illinois at Urbana-Champaign, 1304 West Green Street, Urbana, Illinois 61801

Received August 22, 2003. In Final Form: December 16, 2003

A glucose-sensitive inverse opal hydrogel was synthesized through photopolymerization of 2-hydroxyethyl methacrylate and 3-acrylamidophenylboronic acid within the interstitial space of a dried poly(styrene) colloidal crystal template, followed by template removal. Charged complex formation between the phenylboronic acid functional group and the 1,2-*cis*-diol glucose resulted in reversible swelling of the inverse opal hydrogel, which was observed through shifts in the optical diffraction wavelength. The hydrogel was sensitive to glucose at *physiological* concentrations and ionic strength. The effects of phenylboronic acid concentration, ionic strength, and buffer pH on the equilibrium hydrogel swelling were also studied. The kinetics of hydrogel swelling was also examined, and it was found that the rate of diffraction shift matched well with diffusion-limited kinetics. Additionally, the diffraction response was compared with simulations using the scalar wave approximation and transfer matrix method.

Introduction

There is a growing interest in the creation of optically active 3-D mesostructured hydrogels for chemical and biological sensing. Hydrogels can be designed to undergo reversible changes in physical dimensions in response to external parameters such as solvent composition,[1,2] temperature,[3,4] pH, ionic strength,[5] and biomolecule binding[6−9] through functionalization with responsive moieties. Such reversible swelling makes hydrogels excellent candidate materials for optically based sensors when coupled to an appropriate signal transduction mechanism. One possible method takes advantage of optical diffraction of colloidal crystals arising from their 3-D ordered structure with periodicity on the order of the wavelength of visible light. If the periodicity of the colloidal crystal can be imparted to a responsive hydrogel, then the reversible swelling of the hydrogel may change the periodic spacing, resulting in a shift in diffraction wavelength. For example, if a responsive hydrogel is polymerized in the interstitial space of a colloidal crystal template, the resulting mesostructured hydrogel may form the basis of a sensor based on tunable optical diffraction.

Large area colloidal crystal templates can be formed by self-assembly of monodisperse colloids using techniques including patterned sedimentation,[10] controlled evaporation,[11,12] sonication-assisted packing,[13] formation in a flow cell,[14,15] and other methods.[16] A colloidal crystal formed on a planar substrate usually adapts a face-centered cubic (fcc) structure with the (111) plane parallel to the substrate and interacts strongly with light following Bragg's law:[17]

$$\lambda = 2n_{\text{eff}}d = \frac{2\sqrt{6}}{3}\left(\sum_i n_i^2\phi_i - \sin^2\psi\right)^{1/2}D \qquad (1)$$

where n_{eff} is the effective refractive index from dielectric mixing, d is the interlayer spacing, n and ϕ are respectively the refractive index and the volume fraction of each component phase, ψ is the angle between the incident beam and the sample normal, and D is the diameter of the colloidal template. Colloidal crystals have been successfully utilized to template the growth of mesostructured semiconductors,[12,18,19] metals,[20−22] and various polymers,[23−28] including hydrogels.[15,29−31]

* Corresponding author. E-mail: pbraun@uiuc.edu. Phone: 1-217-244-7293. Fax: 1-217-333-2736.

(1) Tanaka, T.; Fillmore, D.; Sun, S.-T.; Nishio, I.; Swislow, G.; Shah, A. *Phys. Rev. Lett.* **1980**, *45*, 1636−1639.
(2) Katayama, S.; Hirokawa, Y.; Tanaka, T. *Macromolecules* **1984**, *17*, 2643−2645.
(3) Ilavsky, M.; Hrouz, J.; Ulbrich, K. *Polym. Bull.* **1982**, *7*, 107−113.
(4) Hirotsu, S. *J. Chem. Phys.* **1988**, *88*, 427−431.
(5) English, A. E.; Tanaka, T.; Edelman, E. R. *J. Chem. Phys.* **1997**, *107*, 1645−1654.
(6) Kikuchi, A.; Suzuki, K.; Okabayashi, O.; Hoshino, H.; Kataoka, K.; Sakurai, Y.; Okano, T. *Anal. Chem.* **1996**, *68*, 823−828.
(7) Miyata, T.; Asami, N.; Uragami, T. *Nature* **1999**, *399*, 766−769.
(8) Watanabe, M.; Akahoshi, T.; Tabata, Y.; Nakayama, D. *J. Am. Chem. Soc.* **1998**, *120*, 5577−5578.
(9) Anastase-Ravion, S.; Ding, Z.; Pelle, A.; Hoffman, A. S.; Letourneur, D. *J. Chromatogr., B* **2001**, *761*, 247−254.
(10) Braun, P. V.; Zehner, R. W.; White, C. A.; Weldon, M. K.; Kloc, C.; Patel, S. S.; Wiltzius, P. *Adv. Mater.* **2001**, *13*, 721−724.
(11) Jiang, P.; Bertone, J. F.; Hwang, K. S.; Colvin, V. L. *Chem. Mater.* **1999**, *11*, 2132−2140.
(12) Vlasov, Y. A.; Bo, X. Z.; Sturm, J. C.; Norris, D. J. *Nature* **2001**, *414*, 289−293.
(13) Lu, Y.; Yin, Y. D.; Gates, B.; Xia, Y. N. *Langmuir* **2001**, *17*, 6344−6350.
(14) Asher, S. A.; U.S. Patent No. 4627689: Crystalline Colloidal Narrow Band Radiation Filter, 1986.
(15) Asher, S. A.; Holtz, J.; Liu, L.; Wu, Z. J. *J. Am. Chem. Soc.* **1994**, *116*, 4997−4998.
(16) Xia, Y. N.; Gates, B.; Yin, Y. D.; Lu, Y. *Adv. Mater.* **2000**, *12*, 693−713.
(17) Hiltner, P. A.; Krieger, I. M. *J. Phys. Chem.* **1969**, *73*, 2386−2389.
(18) Holland, B. T.; Blanford, C. F.; Do, T.; Stein, A. *Chem. Mater.* **1999**, *11*, 795−805.
(19) Braun, P. V.; Wiltzius, P. *Nature* **1999**, *402*, 603−604.
(20) Jiang, P.; Cizeron, J.; Bertone, J. F.; Colvin, V. L. *J. Am. Chem. Soc.* **1999**, *121*, 7957−7958.
(21) Yang, H. W.; Blanford, C. F.; Lytle, J. C.; Carter, C. B.; Smyrl, W. H.; Stein, A. *Chem. Mater.* **2001**, *13*, 4314−4321.
(22) Bartlett, P. N.; Baumberg, J. J.; Birkin, P. R.; Ghanem, M. A.; Netti, M. C. *Chem. Mater.* **2002**, *14*, 2199−2208.
(23) Park, S. H.; Xia, Y. N. *Adv. Mater.* **1998**, *10*, 1045−1049.
(24) Jiang, P.; Hwang, K. S.; Mittleman, D. M.; Bertone, J. F.; Colvin, V. L. *J. Am. Chem. Soc.* **1999**, *121*, 11630−11637.
(25) Bartlett, P. N.; Birkin, P. R.; Ghanem, M. A.; Toh, C. S. *J. Mater. Chem.* **2001**, *11*, 849−853.

10.1021/la035555x CCC: $27.50
Published on Web 03/10/2004

Scheme 1. Binding Equilibrium between Glucose and the Phenylboronic Acid Group

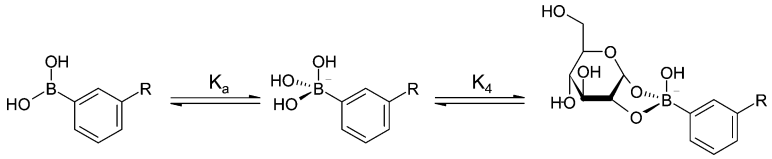

The field of responsive colloidal crystal templated hydrogels is expanding rapidly. The pioneering work of Asher and co-workers generated functional periodic hydrogel structures through polymerization of acrylamide-based aqueous solutions inside charge-stabilized colloidal crystals,[15] followed by modification of the amide group. Using this technique, they and other groups demonstrated colloidal crystal−hydrogel composites termed polymerized colloidal crystal arrays (PCCAs), which exhibited reversible diffraction shifts due to stimuli such as mechanical force,[15,32] complexation between crown ethers and metal ions,[29,30,33] pH and ionic strength,[31] and glucose binding.[30,34,35] A different approach involved the synthesis of colloidal particles of the hydrogel poly(*N*-isopropylacrylamide) (PNIPAM), which were subsequently organized into ordered arrays.[36−39] These periodic structures displayed thermally induced shifts in optical diffraction due to lower critical solution temperature (LCST) behavior. Other groups, including our own, have focused on an inverse opal approach, where a dried colloidal crystal is used to template the polymerization of infiltrated monomer precursors. After polymerization, the colloidal template is removed by chemical etching, yielding a bicontinuous polymer/solvent mesostructure. As an example of this approach, Takeoka and Watanabe polymerized inverse opals consisting of temperature-sensitive PNIPAM, which also showed a reversible diffraction shift versus temperature.[40] We recently synthesized mechanically robust inverse opal hydrogels based on 2-hydroxyethyl methacrylate/acrylic acid (HEMA/AA) copolymers that exhibited optical diffraction sensitive to both pH and ionic strength.[41]

There are certain inherent advantages of both the PCCA and inverse opal based sensor designs. Benefits of the PCCA method include rapid formation of the charge-stabilized colloidal crystal and high diffraction intensity due to large single-crystal domains, both of which are very significant for application. However, because the charge-stabilized colloidal crystal forms only in aqueous-based solutions of very low ionic strength, the hydrogel chemistry is limited to uncharged systems, and incorporation of charged functional groups into the hydrogel requires a second processing step. In addition, to maintain the stability of the charge-stabilized colloidal crystal, the maximum concentration of functional groups that can be introduced may be limited. Finally, the composite PCCA structure does not contain interconnected pores and thus requires the use of low polymer content hydrogels to allow rapid diffusion of analytes, which may limit the mechanical stability of the hydrogel. Advantages of the inverse opal method include the ability to accommodate a wide variety of functional groups and polymerization techniques, the facile variation of functional group concentration, and the ability to polymerize dense, robust hydrogel structures while potentially maintaining connectivity to the bulk solvent. The disadvantages of the inverse opal method include the generally higher defect density of a dried colloidal crystal template and possible damage to the hydrogel mesostructure due to the template etching process using either organic solvent (for polymer colloids) or hydrofluoric acid (for silica colloids).

Functionalized hydrogels are good candidates as sensors for biomolecules due in part to their activity and biocompatibility in aqueous environments. For example, hydrogels functionalized with phenylboronic acid and its derivatives are useful materials for the detection and purification of various carbohydrates.[42] Phenylboronic acid is a Lewis acid that reversibly interacts with 1,2-*cis*-diols such as glucose by forming a charged complex (Scheme 1), where K_a and K_4 are respectively the acid dissociation constant and the equilibrium constant for the binding of glucose to the deprotonated phenylboronic acid. Another equilibrium constant, K_3, exists for the binding of glucose to the uncharged phenylboronic acid, but it is much smaller than K_4.[43]

Binding with glucose causes the charged complex state to be more thermodynamically favorable; in other words, the pK_a of the phenylboronic acid group decreases when bound to a 1,2-*cis*-diol.[44,45] If the phenylboronic acid is covalently attached to a hydrogel, binding to 1,2-*cis*-diols increases the degree of ionization on the hydrogel and builds up a Donnan potential between the hydrogel phase and the bulk solution phase. The resulting influx of solvent and ions leads to hydrogel swelling, which may be detected as a red shift in optical diffraction in a templated hydrogel. The pH of the aqueous solution strongly affects the sensitivity of the functionalized hydrogel to 1,2-*cis*-diols. A higher pH increases the concentration of the deprotonated phenylboronic acid group, which is more sensitive to the analyte due to the larger equilibrium constant, K_4. However, if pH is too high, almost all phenylboronic acid groups become charged, and the additional swelling due

(26) Yoshino, K.; Satoh, S.; Shimoda, Y.; Kajii, H.; Tamura, T.; Kawagishi, Y.; Matsui, T.; Hidayat, R.; Fujii, A.; Ozaki, M. *Synth. Met.* **2001**, *121*, 1459−1462.
(27) Cassagneau, T.; Caruso, F. *Adv. Mater.* **2002**, *14*, 34−38.
(28) Fudouzi, H.; Xia, Y. N. *Adv. Mater.* **2003**, *15*, 892.
(29) Holtz, J. H.; Asher, S. A. *Nature* **1997**, *389*, 829−832.
(30) Holtz, J. H.; Holtz, J. S. W.; Munro, C. H.; Asher, S. A. *Anal. Chem.* **1998**, *70*, 780−791.
(31) Lee, K.; Asher, S. A. *J. Am. Chem. Soc.* **2000**, *122*, 9534−9537.
(32) Foulger, S. H.; Jiang, P.; Lattam, A. C.; Smith, D. W.; Ballato, J. *Langmuir* **2001**, *17*, 6023−6026.
(33) Asher, S. A.; Peteu, S. F.; Reese, C. E.; Lin, M. X.; Finegold, D. *Anal. Bioanal. Chem.* **2002**, *373*, 632−638.
(34) Asher, S. A.; Alexeev, V. L.; Goponenko, A. V.; Sharma, A. C.; Lednev, I. K.; Wilcox, C. S.; Finegold, D. N. *J. Am. Chem. Soc.* **2003**, *125*, 3322−3329.
(35) Alexeev, V. L.; Sharma, A. C.; Goponenko, A. V.; Das, S.; Lednev, I. K.; Wilcox, C. S.; Finegold, D. N.; Asher, S. A. *Anal. Chem.* **2003**, *75*, 2316−2323.
(36) Weissman, J. M.; Sunkara, H. B.; Tse, A. S.; Asher, S. A. *Science* **1996**, *274*, 959−960.
(37) Debord, J. D.; Lyon, L. A. *J. Phys. Chem. B* **2000**, *104*, 6327−6331.
(38) Debord, J. D.; Eustis, S.; Debord, S. B.; Lofye, M. T.; Lyon, L. A. *Adv. Mater.* **2002**, *14*, 658−662.
(39) Hu, Z. B.; Lu, X. H.; Gao, J. *Adv. Mater.* **2001**, *13*, 1708−1712.
(40) Takeoka, Y.; Watanabe, M. *Adv. Mater.* **2003**, *15*, 199−201.
(41) Lee, Y.-J.; Braun, P. V. *Adv. Mater.* **2003**, *15*, 563−566.
(42) James, T. D.; Shinkai, S. *Top. Curr. Chem.* **2002**, *218*, 159−200.
(43) Lorand, J. P.; Edwards, J. O. *J. Org. Chem.* **1959**, *24*, 769−774.
(44) Yoon, J.; Czarnik, A. W. *J. Am. Chem. Soc.* **1992**, *114*, 5874−5875.
(45) James, T. D.; Sandanayake, K. R. A. S.; Shinkai, S. *Angew. Chem., Int. Ed.* **1994**, *33*, 2207−2209.

to glucose binding becomes negligible. Thus, glucose sensing with phenylboronic acid functionalized hydrogels is typically performed at pH ~ pK_a. The pK_a for phenylboronic acid is ~8.8,[46] so a pH between 8.5 and 9.0 is generally used.[6,34]

By exploiting the interaction between phenylboronic acids and 1,2-*cis*-diols, Kataoka and co-workers synthesized a phenylboronic acid functionalized hydrogel that swelled as a function of the glucose concentration in the surrounding solution[6] and, when loaded with insulin, released insulin upon exposure to glucose.[47] A similar hydrogel copolymerized from phenylboronic acid and NIPAM was utilized as a separation agent for RNA by binding to the ribose group on the RNA backbone.[48] Asher and co-workers synthesized a PCCA of a phenylboronic acid functionalized hydrogel which exhibited a diffraction shift in solutions containing various carbohydrates, and they extrapolated the equilibrium constants for sugar binding by fitting the diffraction shift to the swelling theory of cross-linked polyelectrolytes.[34] Interestingly, they noted that the PCCA diffraction response ceased for ion concentrations of >10 mM, apparently due to the weakening of the Donnan potential in high ionic strength solutions. More recently, they also demonstrated a PCCA which contracted after introduction of glucose due to increased cross-linking caused by the binding of each glucose molecule to two pendant phenylboronic acid groups.[35]

In this report, we created inverse opal glucose-sensitive hydrogels through copolymerization of 3-acrylamidophenylboronic acid (APBA) and 2-hydroxyethyl methacrylate (HEMA) inside a dried poly(styrene) colloidal crystal template followed by etching and solvent exchange. The inverse opal hydrogel film was enclosed in a microfluidic flow cell (Figure 1a) to facilitate the transport of molecules between the bulk solution and the hydrogel. To investigate diffraction from a single or few domains of the inverse opal hydrogel, a microspectrometer consisting of an inverted reflection microscope with output coupled to a fiberoptic spectrophotometer was used. The equilibrium and kinetic swelling behavior of the hydrogel sensors versus glucose concentrations at physiological ionic strength were determined from the reflection spectra. The effects of APBA concentration, ionic strength, and solution pH on the magnitude of diffraction shift were also examined. We found that the APBA-functionalized inverse opals exhibited reversible glucose binding induced diffraction shifts of ~5 nm/mM glucose at physiological glucose concentrations (~5 mM) and ionic strength (150 mM). The kinetics of the diffraction shift followed a pseudo-diffusion-limited relationship, and the equilibration time decreased at higher glucose concentrations, suggesting that as expected, the diffusivity of glucose in the hydrogel increased as the hydrogel became more swollen. Finally, the diffraction response was compared with theoretical results calculated using the scalar wave approximation (SWA)[49] and the transfer matrix method (TMM),[50,51] using simple models for the swelling of the mesoporous hydrogel.

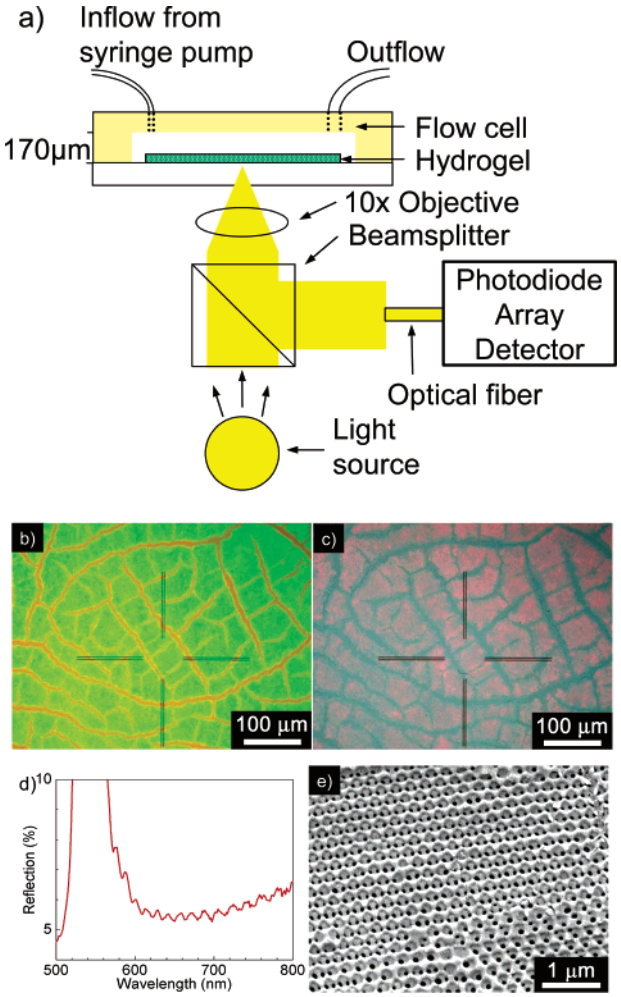

Figure 1. (a) Schematic for microspectroscopy of a flow cell containing an inverse opal hydrogel. A flow cell was constructed from patterned PDMS and a glass substrate, minimizing the amount of analyte solution needed while maintaining laminar flow. Light reflected from the sample was collected by the objective and fiberoptically coupled to the spectrophotometer. (b) Optical reflection micrograph of a 6.25% APBA templated hydrogel in DI water. Strong diffraction of green light was generally observed, and opaque lines corresponding to drying cracks in the colloidal template were seen, indicating an average domain size of ~30 μm. Each reflection spectrum was collected from the region at the center of the crosshairs. (c) Optical reflection micrograph of the same hydrogel after exposure to 1 mM glucose in pH 9 buffer for ~20 min. (d) Reflection spectrum of a 6.25% APBA hydrogel in DI water, showing the Fabry–Perot fringes due to interfacial interference. (e) SEM of the 6.25% APBA hydrogel (top view), showing the expected fcc-(111) inverse opal structure with a pitch of ~240 nm.

Experimental Section

Materials. An 8% v/v aqueous suspension of 244 nm ± 7 nm diameter monodisperse sulfate-terminated poly(styrene) colloids (1-200, Interfacial Dynamics Co., Portland, OR) was used to form the colloidal template. 3-Aminophenylboronic acid hemisulfate (Acros), acrylic acid (Acros), 1-ethyl-3-(3-dimethylaminopropyl)-carbodiimide hydrochloride (EDC) (Pierce Biotechnology, Inc., Rockford, IL), methacryloxypropyltrimethoxysilane (MPMS) (Gelest, Inc., Tullytown, PA), (tridecafluoro-1,1,2,2-tetrahydrooctyl)dimethylchlorosilane (FDCS) (Gelest, Inc.), HEMA (Sigma-Aldrich), ethylene glycol dimethacrylate (EGDM) (Sigma-Aldrich), Irgacure 651 photoinitiator (IR-651) (Ciba Specialty Chemicals, Inc., Basel, Switzerland), 2-(cyclohexylamino)ethanesulfonic acid (CHES) (Acros), D(+)-glucose (Acros), and 1,2-*cis*-cyclohexanediol (Acros) were used as received. Forty-eight gauge Mylar EL films (12 μm) for spacers were generously supplied by Dupont Teijin Films. Milli-Q deionized (DI) water

(46) Barker, S. A.; Chopra, A. K.; Hatt, B. W.; Somers, P. J. *Carbohydr. Res.* **1973**, *26*, 33–40.
(47) Kataoka, K.; Miyazaki, H.; Bunya, M.; Okano, T.; Sakurai, Y. *J. Am. Chem. Soc.* **1998**, *120*, 12694–12695.
(48) Elmas, B.; Onur, M. A.; Senel, S.; Tuncel, A. *Colloid Polym. Sci.* **2002**, *280*, 1137–1146.
(49) Mittleman, D. M.; Bertone, J. F.; Jiang, P.; Hwang, K. S.; Colvin, V. L. *J. Chem. Phys.* **1999**, *111*, 345–354.
(50) Pendry, J. B.; Mackinnon, A. *Phys. Rev. Lett.* **1992**, *69*, 2772–2775.
(51) Bell, P. M.; Pendry, J. B.; Moreno, L. M.; Ward, A. J. *Comput. Phys. Commun.* **1995**, *85*, 306–322.

(Millipore) was used for the experiments. pH measurements were taken using a Accumet AR-10 pH meter (Fisher Scientific). Sonication was performed on a Fisher F530 sonicator (Fisher Scientific).

Optical Spectrocopy. Light reflected from the sample was collected by a 10× objective (NA = 0.25) on an inverted optical microscope (Axiovert 135, Carl Zeiss Inc.) and fiberoptically coupled to a diffraction grating photodiode array detector (PDA-512, Control Development, Inc., South Bend, IN) to collect the reflection spectra in the sample normal direction. The 400 μm core diameter of the optical fiber limits the analysis area to ~10 μm^2 at the center of the image area.

APBA Synthesis. APBA was synthesized in a procedure similar to that of Kitano and co-workers.[52] In a 100 mL round-bottom flask, 3-aminophenylboronic acid hemisulfate (1.862 g, 10 mmol) was dissolved in water (30 mL), and the pH of the solution was adjusted to 4.8 by adding NaOH. The flask was stirred in an ice bath, and after temperature equilibration, EDC (2.301 g, 12 mmol) was added, and the pH was again adjusted to 4.8. In another container, acrylic acid (0.868 g, 12 mmol) was dissolved in water (10 mL), followed by pH adjustment to 4.8. The acrylic acid solution was then slowly added to the flask, and the mixture was capped with a rubber septum and allowed to stir in an ice bath for 1 h. The flask was then removed from the ice bath and left at room temperature overnight. The reaction mixture was extracted with 4× ethyl ether and rotovaped (R-114, Buchi). The resulting oily liquid was mixed with water (30 mL) and stirred in the ice bath for 24 h, leading to precipitation of needlelike crystals. The solid precipitate was collected by filtration (no. 1, Whatman). FTIR (Nexus 670, Thermo Nicolet) showed absorption maxima at 1340 cm^{-1} (B−O), 1550 cm^{-1} (−CONH−), and 1660 cm^{-1} (−CONH−). ^{1}H NMR spectroscopy in CD_3OD was performed in a Varian UNITY 300 NMR spectrometer and showed chemical shifts at $\delta = 5.8$ (1H, CH_2═CH−), $\delta = 6.4$ (2H, CH_2═CH−), and $\delta = 7.2-7.8$ (4H, phenyl). The overall yield was 48%.

Colloidal Template Formation. The colloidal crystals were formed using a method adapted from Xia and co-workers.[13] Glass slides (25 mm × 25 mm) were cut from standard microscope slides (12-544-1, Fisher Scientific) and used as bottom slides. Holes (2.5 mm diameter) were drilled through some of the glass slides using a diamond-tipped drill bit (Micromite Diamond Glass Drill, Lapcraft, Inc., Powell, OH) for use as top slides. All slides were then cleaned using a mixture of glassware cleaning agent (Nochromix, Godax Laboratories, Inc., Takoma Park, MD) and sulfuric acid for 12 h, rinsed with DI water, submerged in 5% v/v HF for 15 s, rinsed again with DI water, and dried under flowing N_2. Top slides were submerged in 2 mM FDCS in toluene for 10 min to render them hydrophobic. Bottom slides were submerged in 2 mM MPMS in acetone for 10 min to functionalize the surface with acrylate groups. Glass tubes (5 mm inside diameter, 25 mm length) were attached to a top slide via 5 Minute Epoxy (Devcon, Danvers, MA) to form a reservoir. Spacers were made by cutting 15 mm × 15 mm square holes inside 25 mm × 25 mm × 12 μm Mylar films and cleaned by sonication in ethanol. Each spacer was submerged in a 0.05% v/v poly(styrene) colloidal suspension in ethanol for 30 s. A cell was assembled by clamping together a bottom slide, a colloid decorated spacer, and a top slide/reservoir with binder clips. Aqueous poly(styrene) colloidal suspension (300 μL, 2% v/v) was injected into the reservoir and capped tightly with a standard rubber pipet bulb. Two strips of duct tape were affixed on top of the sonicator across the two diagonals. The assembled cell was placed on the edge of a glass Petri dish on top of the tape so that the slide formed a 30° angle to horizontal. After 24 h of sonication, the cell was removed from the sonicator, excess colloidal suspension was decanted, and the cell was allowed to dry overnight under a covered crystallization dish.

Inverse Opal Hydrogel Synthesis. Mixtures of phenylboronic acid, cross-linker, and photoinitiator were dissolved in the monomer and infiltrated into the colloidal crystal template for UV polymerization. For the 6.25% APBA sample, APBA (90.7 mg, 475 μmol), EGDM (15.0 mg, 75.7 μmol), and IR-651 (19.7 mg, 75.7 μmol) were dissolved in HEMA (0.916 g, 7.04 mmol). For the 1.25% APBA sample, a different amount of APBA (18.4 mg, 95.5 μmol) was used. For the control sample, only EDGM and IR-651 were added to HEMA. For each sample, ~300 μL of the mixture was pipetted into the injection tube, which was then capped with a pipet bulb. Once the colloidal crystal became translucent, indicating successful infiltration, excess precursors were removed from the injection tube, and the remaining mixture was photopolymerized at 365 nm for 50 min using a high-intensity UV lamp (B-100A, UVP, Inc., Upland, CA). The two slides were separated and then placed in chloroform for at least 24 h to fully dissolve the poly(styrene) colloids. The inverse opal hydrogel typically stayed on the bottom slide. Each inverse opal hydrogel was solvent exchanged by submerging the sample in 50% v/v ethanol in chloroform for 60 s, then in pure ethanol for 60 s, then in 50% v/v ethanol in water for 60 s, after which it was placed in water for storage.

Scanning Electron Microscopy. After template etching, an inverse opal hydrogel was removed from chloroform, dried in air, and characterized by scanning electron microscopy (SEM) (Philips XL30 ESEM-FEG).

Fabrication of Microfluidic Cell. A seal was made from patterned poly(dimethylsiloxane) (PDMS)[53] formed by pouring mixed and degassed PDMS prepolymer (Sylgard 184, Dow Corning Co., Midland, MI) over a precleaned 18 mm × 18 mm no. 1 cover slip placed on top of a standard 2 in. Si wafer in a poly(styrene) Petri dish and cured at 70 °C for 1 h. The cover slip/Si wafer was detached from the cured PDMS, and a ~3 cm × 3 cm block was cut from the cured polymer to yield PDMS with an indentation of 18 mm × 18 mm × 170 μm at the center. A small hole was bored through the PDMS at one corner of the indentation using a disposable 20-gauge needle polished by 120-grit sandpaper to remove the anticoring tip. A larger hole was bored at the adjacent corner using a similarly polished disposable 16-gauge needle. A ~3 cm long 26-gauge Teflon tubing ("inlet") was coated on one end with a thin layer of PDMS prepolymer, taking care not to coat the inside of the tube, and was inserted into the small hole until the tip was flush with the indentation. In a similar fashion, a ~20 cm long 20-gauge Teflon tubing ("outlet") was coated and inserted into the larger hole. The assembled PDMS block was cured at 70 °C for 1 h to form the seal.

Characterization of Diffraction Response by Reflection Spectroscopy. For diffraction response experiments, 75 mM CHES buffer solution (ionic strength ~ 150 mM) at pH 9 was made by mixing CHES (1.555 g, 7.5 mmol) and NaCl (0.707 g, 12 mmol) in DI water to make a 50 mL solution, followed by addition of 1 M NaOH (2.502 g) and dilution to 100 mL with DI water. CHES buffer solutions at pH 9.5 and pH 7.4 were made in the same fashion, except the amount of 1 M NaOH was varied. Glucose was then added to yield concentrations ranging from 0.1 to 100 mM. For ionic strength tests, pH 9 buffer solutions of 75 mM CHES buffer solution containing 10 mM glucose and 0−300 mM NaCl were used. Each buffer was drawn into a disposable syringe. A bottom slide containing the inverse opal hydrogel was removed from the storage solution. Excess liquid on the areas not containing the hydrogel was carefully wicked away. The PDMS seal was aligned with the slide by hand, and the edges of the seal and the glass slide were firmly pressed together to form the flow cell. The cell was then manually filled with DI water through the inlet tube. The reflectance from a front-silvered mirror (02 MFG 015/038, Melles Griot, Irvine, CA) with absolute reflectance of ≥95% (400 nm to 20 μm) was used as the reference. The syringe containing the appropriate buffer solution was placed in a syringe pump (Sage M365, Thermo Electron Co., Beverly, MA) and connected to the flow cell inlet with ~30 cm of 26-gauge Teflon tubing. A solution flow rate of 2.5 μL per second was used during testing, and the reflection spectra were collected by the microspectrometer software.

Peak Analysis and Simulation. Diffraction wavelength, full width at half-maximum (fwhm), and peak intensity values for the 6.25% APBA inverse opal film during equilibrium and kinetics tests were determined by curve fitting with Origin 7.0 (OriginLab Co., Northampton, MA) using a Pearson VII fit. To calculate the

(52) Kitano, S.; Koyama, Y.; Kataoka, K.; Okano, T.; Sakurai, Y. *J. Controlled Release* **1992**, *19*, 161−170.

(53) McDonald, J. C.; Whitesides, G. M. *Acc. Chem. Res.* **2002**, *35*, 491−499.

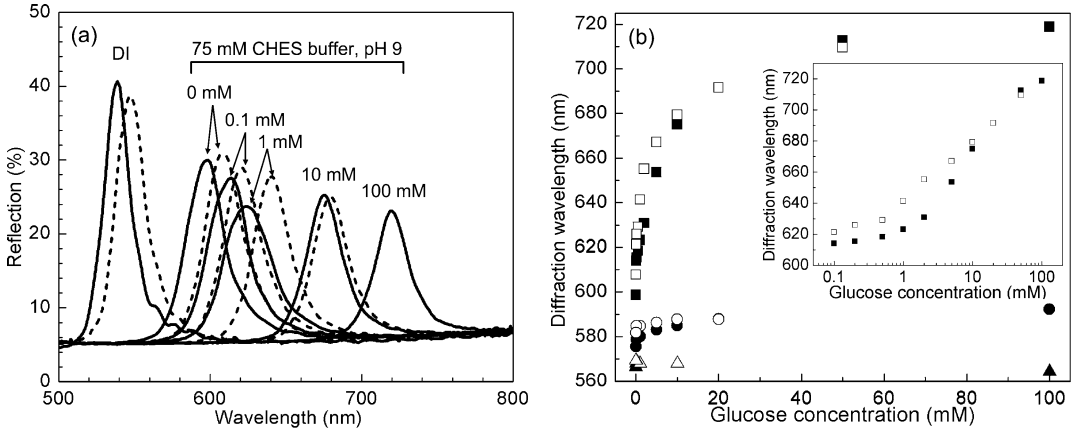

Figure 2. (a) Reflection spectra of a 6.25% APBA hydrogel at selected glucose concentrations, showing a red shift in diffraction due to change in both pH (DI water to pH 9) and glucose concentration (0−100 mM). Solid lines correspond to increasing glucose concentration, and dashed lines correspond to decreasing glucose concentration. (b) Diffraction response dependence on glucose concentration for inverse opal hydrogels with different APBA concentrations. Solid symbols correspond to increasing glucose concentration, and open symbols correspond to decreasing glucose concentration. Squares, 6.25% APBA; circles, 1.25% APBA; triangles, 0% APBA (control film). Inset: Semilog plot of diffraction wavelength vs glucose concentration for 6.25% APBA hydrogel. The greatest response to glucose is at 1−10 mM, which is close to physiological concentrations (∼5 mM).

theoretical diffraction peak, we formulated three simple models of hydrogel swelling which differed in how the fcc pores change dimensions. The refractive index of the polymer (n_{poly}) was approximated using the published value for poly(HEMA) (n = 1.5119).[54] The refractive index values for the aqueous solutions (n_{aq}) were measured by refractometry (Abbe-3L, Fisher Scientific). The effective refractive index of the swollen hydrogel phase (n_{gel}) was calculated using the dielectric mixing rule stated in eq 1, with the assumption that any change in the volume of the hydrogel phase was caused entirely by the influx of the aqueous solution with refractive index of n_{aq}. The new interlayer spacing was also calculated using eq 1. The SWA calculation of peak intensity and normalized fwhm were performed using IDL 5.6 software (Research Systems, Inc., Boulder, CO) using published equations.[49] The transfer matrix simulation of reflection spectra was performed using Translight, a freely available software written by A. L. Reynolds.[55] The calculated peak values were then compared to fitted experimental peak values.

Results

Optical Properties of Inverse Opal Hydrogels. A reflection optical micrograph of the 6.25% APBA hydrogel in pH 6 phosphate buffer is shown in Figure 1b. The templated film generally exhibited good single-color diffraction. The expected drying cracks in the original colloidal template are clearly visible as jagged lines separating irregularly shaped single-crystal domains with an average length of ∼30 μm. The corresponding reflection spectrum has an initial diffraction wavelength λ_0 of 539 nm (Figure 2a). In deionized water, the 1.25% APBA hydrogels and a control hydrogel containing no APBA also exhibited the same initial diffraction wavelength within ∼5 nm (data not shown). Substituting the value of λ_0 along with the refractive indices of DI water (n = 1.3328) and PHEMA (n = 1.5119) into eq 1, assuming an inverse fcc hydrogel structure, resulted in D = 239 nm, which was in agreement with the diameter of the colloid (244 ± 7 nm). Closer examination of the spectrum (Figure 1d) revealed the presence of closely spaced Fabry−Perot interference fringes due to constructive interference of reflections from the top and bottom surfaces of the 3-D hydrogel structure. We calculated the thickness of the inverse opal from the wavelengths of the fringe maxima[49] and found the value to be 10.3 μm, or ∼52 layers of fcc-(111) water spheres in a poly(HEMA) matrix. The color of diffracted light changed from green to red when 1 mM glucose in pH 9 CHES buffer was introduced (Figure 1c), indicative of hydrogel swelling.

Glucose Sensing with APBA-Functionalized Hydrogels. The diffraction spectra of the 6.25% APBA hydrogel in buffer solutions of various glucose concentrations collected from an area of ∼10 μm^2 are plotted in Figure 2a. As expected, the optical diffraction red shifted as glucose concentration increased (solid line), due to the increase in interlayer spacing as the concentration of the anionic APBA−glucose complex increased. The diffraction wavelength then blue shifted when glucose concentration was decreased (dashed line). To quantify the effect of glucose concentration on the swelling of the inverse opal hydrogels, the diffraction wavelengths for hydrogels containing 6.25, 1.25, or 0 mol % APBA are shown in Figure 2b. As previously mentioned, the 6.25% APBA hydrogel diffracted 539 nm light when initially submerged in DI water (pH ∼ 6). When pH 9 buffer with an ionic strength of 150 mM was introduced, the diffraction wavelength increased to 599 nm due to deprotonation of the acid moieties. The increase in diffraction wavelength corresponds to a diffraction shift due to acid deprotonation $(\lambda/\lambda_0)_a$ of 1.111. Increasing the glucose concentration at pH 9 resulted in a gradual red shift of the diffraction wavelength until it reached 719 nm at 100 mM glucose, leading to a total shift (λ/λ_0) of 1.334. The diffraction shift due to phenylboronic acid−glucose binding, $(\lambda/\lambda_0)_b$, is then equal to $(\lambda/\lambda_0)/(\lambda/\lambda_0)_a$ = 1.201. The diffraction red shift was also easily perceptible to the naked eye, as the hydrogel film changed from a yellow-orange color at 0 mM glucose to clear (diffracting in the infrared) at 100 mM glucose. Thus, even at physiological ionic strength, the APBA-functionalized inverse opal hydrogel film exhibited sensitivity to glucose that was easily detected both spectroscopically and visually. The diffraction response of the 1.25% APBA hydrogel at different glucose concentrations is also shown in Figure 2b. A reversible red shift in diffraction wavelength was observed, going from 539 nm in DI water (not shown), to 575 nm in 0 mM glucose at pH 9, to 592 nm in 100 mM glucose at pH 9, leading to a $(\lambda/\lambda_0)_b$ of 1.030. In contrast, the control sample showed no sensitivity to glucose. Replacing DI water with pH 9

(54) Brandrup, J.; Immergut, E. H.; Grulke, E. *Polymer Handbook*; Wiley: New York, 1999.

(55) Reynolds, A. L.; Arnold, J. M. Available at http://www.elec.gla.ac.uk/groups/opto/photoniccrystal/Software/SoftwareMain.htm.

Table 1. Diffraction Wavelength and Peak Intensity of 6.25% APBA Hydrogel at Various pHs for Increasing and Decreasing Analyte Concentration

analyte	solvent	[analyte] (mM)	λ_{inc}[a] (nm)	I_{inc}[a] (%)	λ_{dec}[b] (nm)	I_{dec}[b] (%)
glucose	DI water	0	539	35.7	548	33.2
	pH 9 buffer	0	599	24.4	608	25.5
	pH 9 buffer	100	719	17.1		
glucose	DI water	0	540	32.3	542	33.4
	pH 7.4 buffer	0	597	26.1	600	25.0
	pH 7.4 buffer	100	603	24.9		
glucose	DI water	0	531	20.4	540	19.3
	pH 9.5 buffer	0	666	9.5	673	8.6
	pH 9.5 buffer	100	718	5.4		
cis-1,2-cyclo-hexanediol	DI water	0	542	36.3	547	36.8
	pH 9 buffer	0	617	20.0	620	21.2
	pH 9 buffer	100	634	19.7		

[a] Data collected during increasing analyte concentration. [b] Data collected during decreasing analyte concentration.

buffer caused the diffraction wavelength to red shift from 533 nm (not shown) to 566 nm (Figure 2b), which may be explained by the presence of an acrylic acid impurity in as-received HEMA.[56] The hypothesis is supported by gas chromatography of as-received HEMA, which revealed the presence of acrylic acid at a concentration of ~0.15 mol %. Increasing the glucose concentration to 100 mM at pH 9 caused the diffraction wavelength of the control film to shift to 565 nm, which corresponds to a slight shrinkage of the hydrogel when the increase in refractive index from a 0−100 mM glucose solution (~1%) was taken into account. Thus, the diffraction red shift observed in APBA-functionalized hydrogels at pH 9 must be caused by complex formation between glucose and APBA.

Two interesting trends were observed in the optical response of the APBA-functionalized hydrogels to glucose. First, the diffraction peak intensity values decreased monotonically as the hydrogel swelled (Figure 2a), with one exception that may be caused by a small shift in sampling spot during data collection. This behavior was observed in all samples (Table 1). The inverse relationship between diffraction peak intensity and diffraction shift of the hydrogel may be explained by a number of causes including a decrease in refractive index contrast during film swelling, an increasing presence of disorder in a swollen hydrogel, or partial pore closure during hydrogel expansion, which we will discuss in more detail later. At the same time, the general shape of the peaks remains unchanged, suggesting that the overall layered mesostructure of the templated hydrogel was maintained during swelling. Second, while diffraction response appeared to reach steady state during the time frame of the experiment (~20 min between data points in Figure 2b), the diffraction wavelengths during decreasing glucose concentration (open symbols) are red shifted versus their counterparts during increasing glucose concentration (solid symbols). This hysteresis completely disappeared after soaking the hydrogel film overnight, suggesting the existence of very slow kinetics in some portion of the inverse opal hydrogel.

pH and Analyte Effects. As described in the Introduction, the pH of the glucose solution may significantly affect the degree of swelling of the APBA-functionalized hydrogel and therefore control the diffraction response. Indeed, when the pH of the buffer was adjusted to 7.4, the 6.25% APBA hydrogel became almost completely insensitive to glucose. Its diffraction wavelength changed from 597 nm in 0 mM glucose to 603 nm in 100 mM glucose

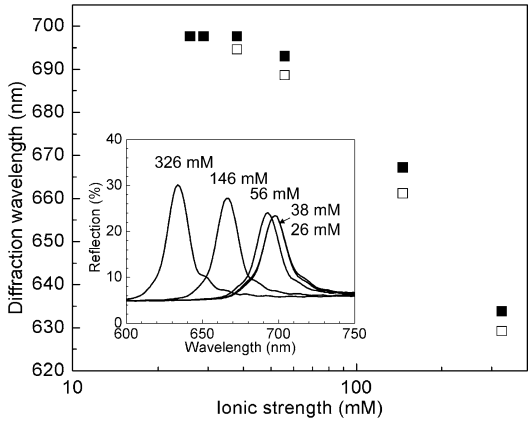

Figure 3. Effect of ionic strength on diffraction response of 6.25% APBA hydrogel in 10 mM glucose solution. A red shift of diffraction from 634 to 699 nm was observed when the ionic strength was reduced from 326 to 38 mM (solid squares), at which point the response became saturated. Increasing the ion concentration caused the diffraction wavelength to blue shift to 628 nm (open squares). Inset: reflection spectra of 6.25% APBA hydrogel at several ionic strengths.

(Table 1), corresponding to zero swelling after accounting for the change in solution refractive index. A similar lack of response at physiological pH for the low ionic strength PCCA glucose sensor was reported.[34] However, when the pH of the buffer was changed to 9.5, we found that the diffraction response of the hydrogel to glucose was diminished but still detectable. The diffraction wavelength red shifted from 531 nm in DI water, to 666 nm in 0 mM glucose at pH 9.5, to 718 nm in 100 mM glucose at pH 9.5 (Table 1). The corresponding $(\lambda/\lambda_0)_b$ is 1.078. This behavior is different than that of the low ionic strength PCCA glucose sensor, which exhibited no response at pH 9.5.[34] The 6.25% APBA hydrogel was also responsive to *cis*-1,2-cyclohexanediol, an analogue of glucose which (unlike glucose) does not undergo mutarotation (cis−trans isomerization). The diffraction wavelength red shifted from 542 nm in DI water, to 617 nm in 0 mM *cis*-1,2-cyclohexanediol at pH 9, to 634 nm in 100 mM *cis*-1,2-cyclohexanediol at pH 9. The corresponding $(\lambda/\lambda_0)_b$ is 1.028, suggesting that APBA binding to *cis*-1,2-cyclohexanediol is less favorable than to glucose. Finally, a similar hysteresis in diffraction wavelength between decreasing and increasing analyte concentration was observed for all hydrogel samples that swelled.

Ionic Strength Dependence of Diffraction Response. By varying the concentration of NaCl in pH 9 CHES buffer solutions containing 10 mM glucose, the effect of ionic strength on diffraction response was studied and plotted in Figure 3. The ionic strength of a 75 mM buffer solution of CHES (pK_a = 9.3) at pH = 9 was estimated to be 26 mM and was added to the NaCl concentration to calculate the total ionic strength.[57] As expected for a system where hydrogel swelling was caused by an increase in the Donnan potential due to ionization, the diffraction response of the 6.25% APBA hydrogel to 10 mM glucose became more pronounced as ionic strength was decreased. The diffraction wavelength red shifted from 634 nm at an ionic strength of 326 mM to 698 nm at an ionic strength of 38 mM, after which it remained constant as the ionic strength decreased further to 26 mM (Figure 3). When the ionic strength was returned to 326 mM, the diffraction wavelength blue shifted to 628 nm. Thus, our inverse opal hydrogel exhibited diffractive optical response

(56) Mayes, A. G.; Blyth, J.; Millington, R. B.; Lowe, C. R. *Anal. Chem.* **2002**, *74*, 3649−3657.

(57) Perrin, D. D.; Dempsey, B. *Buffer for pH and Metal Ion Control*; Chapman and Hall: London, 1974.

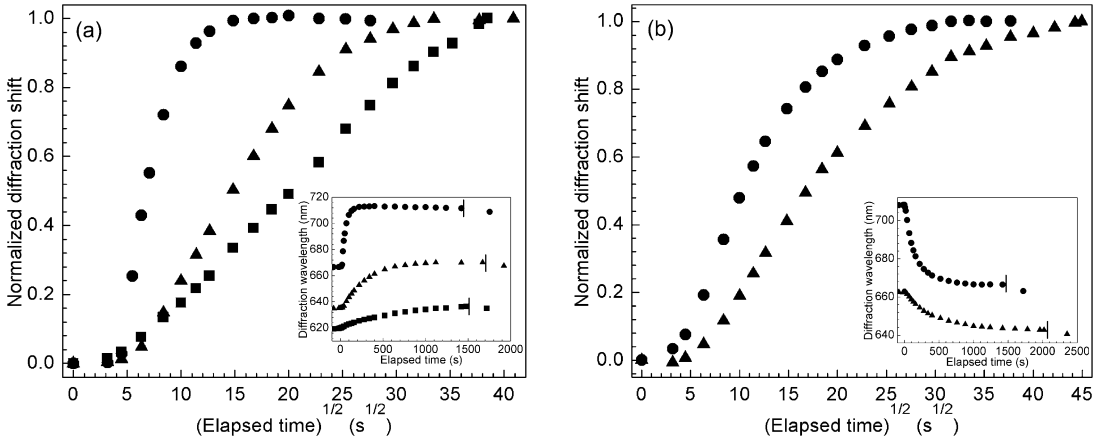

Figure 4. Kinetics of glucose sensing for 6.25% APBA hydrogel. (a) Normalized diffraction response for increasing glucose concentration. Squares, 0.1 to 1 mM; triangles, 1 to 10 mM; circles, 10 to 100 mM. (b) Normalized diffraction response for decreasing glucose concentration. Circles, 100 to 10 mM; triangles, 10 to 1 mM. Insets of both graphs: diffraction wavelength as a function of elapsed time. The vertical black line marks the time when the pump was turned off and flow stopped.

to glucose at physiological (∼150 mM) and even greater ionic strengths, and ionic strength had little effect below ∼40 mM. In comparison, the low ionic strength PCCA glucose sensor reported by Asher and co-workers, which employs the same phenylboronic acid based glucose sensing mechanism, demonstrated good sensitivity to glucose at ∼2 mM ionic strength, which disappeared when ionic strength was increased above 10 mM.[34] We believe the ability of the inverse opal hydrogel to maintain sensitivity to glucose at high ionic strength may be attributed to the higher concentration of functional groups that can be attached to a dense hydrogel versus the dilute hydrogel PCCA structure.

Diffraction Response Kinetics. The kinetics of the diffraction shift due to phenylboronic acid−glucose binding was examined by studying the time evolution of diffraction wavelength inside a microfluidic flow cell. With flow cell dimensions of 1.8 cm × 1.8 cm × 170 μm, a flow rate of 2.5 μL/s is equivalent to a Reynolds number Re ∼ 15.3,[58] so the flow of glucose solution above the inverse opal hydrogel was approximately laminar. By fluorescence microscopy with a rhodamine dye solution, we found that ∼80 s is required for the solution front to be pumped from the syringe to the microfluidic flow cell, and this lag was subtracted from the recorded time to yield the actual elapsed time. The time evolution of the diffraction wavelength was recorded for three stepwise changes in glucose concentration at pH 9: 0.1 to 1 mM, 1 to 10 mM, and 10 to 100 mM (Figure 4a, inset). For all three concentration increases, the diffraction wavelength red shifted gradually for ∼10 s and then increased rapidly until it approached an equilibrium value. In all cases, when the flow was stopped, the diffraction wavelengths decreased ∼2 nm to their final equilibrium value. To clarify the nature of the diffraction response kinetics, the diffraction wavelength values were normalized to their steady-state values before the flow was stopped and plotted versus the square root of elapsed time t (Figure 4a). In all three cases, a single straight line could be fit to the data for the majority of each experimental run, suggesting that the kinetics was proportional to $t^{1/2}$, which is characteristic of a diffusion-limited process. For the two stepwise decreases in glucose concentration (100 to 10 mM and 10 to 1 mM), the diffraction shift kinetics followed the same $t^{1/2}$ relationship (Figure 4b).

For the change from 0.1 to 1 mM glucose, the diffraction shift began to slow at $t \sim 1000$ s but did not flatten completely during the time of the experiment, with an equilibration time of ≥1500 s. When glucose concentration was increased from 1 to 10 mM, a similar $t^{1/2}$ dependence was found (Figure 4a, triangles). The diffraction shift began to slow at $t \sim 500$ s, and equilibrium was reached at $t \sim 1100$ s. For 10 to 100 mM, even faster kinetics was observed (Figure 4a, circles); the slow swelling regime was reached at $t \sim 100$ s, and by $t \sim 250$ s the diffraction wavelength had reached its equilibrium value. Decreasing glucose concentration resulted in diffraction blue shifts with slower rates than when glucose concentration was increased (Figure 4b). For example, an equilibration time of ∼1000 s was found for 100 to 10 mM, and the equilibration time was ≥2100 s when glucose concentration dropped from 10 to 1 mM. The apparent diffusivity of glucose in the dense hydrogel, D_{app}, can be estimated from pseudo 1-D diffusion, using the diffusion equation $x^2 = 2D_{app}t$, where x is the film thickness (10.3 μm) and t is the equilibration time. From the equilibration time values, it was found that D_{app} ranged from 2.5×10^{-10} to 2×10^{-9} cm^2/s, which is much smaller than the diffusivity of glucose in water, 6.7×10^{-6} cm^2/s.[59] Since the HEMA monomer mixture used in photopolymerization contained no water, the value of D_{app} is expected to be low initially and then increase as the volume fraction of water in the hydrogel phase increases due to glucose binding, consistent with the result of Figure 4. Removal of ∼1−2 μm of hydrogel film by exposure to oxygen plasma did not appreciably change the kinetics of diffraction response, although the diffraction intensity was lowered compared to untreated samples, indicating the kinetics are not a function of the structure at the film−fluid interface (Supporting Information: Part B).

Analysis of Reflection Spectra. Peak analysis was performed on the reflection spectra of the 6.25% APBA hydrogel in different glucose concentrations to determine the effect of hydrogel swelling on the optical response and if the templated hydrogel structure becomes disordered upon swelling. The best-fit diffraction intensity and normalized fwhm in % (fwhm divided by diffraction wavelength × 100) for the 6.25% APBA hydrogel were plotted against diffraction shift (λ/λ_0) and displayed in Figure 5. The diffraction intensity decreased monotonically

(58) Bird, R. B.; Stewart, W. E.; Lightfoot, E. N. *Transport Phenomena*; John Wiley and Sons: New York, 1960.

(59) *CRC Handbook of Chemistry and Physics*, 74th ed.; CRC Press: Boca Raton, FL, 1993.

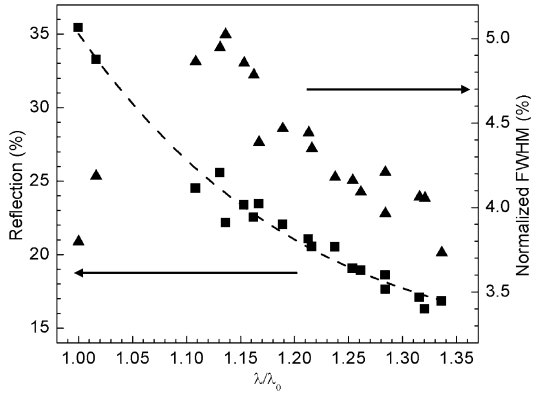

Figure 5. Curve fit data of reflection peak intensity (squares) and normalized fwhm (triangles) for the 6.25% APBA hydrogel versus diffraction shift (λ/λ_0) due to pH change and glucose binding. The dashed line is a guide for the eye.

as the templated hydrogel swelled, going from 35% to 17% as the hydrogel expanded from $\lambda/\lambda_0 = 1$ (DI water) to $\lambda/\lambda_0 = 1.34$ (100 mM glucose). The normalized fwhm exhibited a complex behavior versus diffraction shift which seems to be sensitive to variations in the hydrogel mesostructure, as shown by the scatter in their values at different diffraction shifts (Figure 5). Indeed, reflection data from a different sample with the same composition showed the same decrease in diffraction intensity versus diffraction shift, but the normalized fwhm values did not appear to be a function of hydrogel swelling (Supporting Information: Part B). In summary, the trend in diffraction intensity as a function of diffraction shift was consistent across multiple points on multiple samples, while the normalized fwhm had a less obvious relationship to diffraction shift.

Using the diffraction wavelength of the 6.25% APBA hydrogel as the starting point, we calculated the expected diffraction peak intensity and normalized fwhm values of an inverse opal hydrogel during swelling. To determine the effects of varying refractive index contrast and pore shrinkage on the reflection spectra, three simple models of hydrogel swelling were used. All three models assumed that the film swelled macroscopically in the sample normal direction with aqueous solution at the given pH and glucose concentration; however, the fcc pores change dimensions in different ways (Figure 6a). In the 0-D pore swelling model, the fcc pores maintain their shape and volume during hydrogel swelling, so the volume fraction of pores decreases. In the 1-D pore swelling model, the fcc pores swell in the same 1-D fashion as the bulk film, resulting in a constant pore volume fraction (~0.74) during hydrogel swelling. In the 2-D pore shrinkage model, the hydrogel swells into the pores, causing the pores to shrink in the directions parallel to the substrate. The diffraction wavelength values from six experimental reflection spectra were substituted into eq 1 to calculate the refractive indices and volume fractions of the component phases and interlayer spacing of the hydrogel at each swelling state (for details, see Supporting Information: Part A).

These optical constants and structures for the hydrogel were used to predict its reflection spectra using two methods. In the SWA method, the full Maxwell equations are approximated by scalar equivalents; one such approximation for the fcc photonic crystal probed in the [111] direction has been reported previously.[49] Using the refractive indices, volume fractions, and interlayer spacing as the input, we implemented the approximation in IDL to derive the simulated reflection spectrum for each swelling state, from which the diffraction intensity and normalized fwhm can be extracted. For the TMM simulation,[50,51] given the unit cell of the 3-D mesostructure for the hydrogel at a given swelling state, the corresponding reflection spectrum was simulated with a freely available software.[55] For ease of calculation, an inverse opal of 24

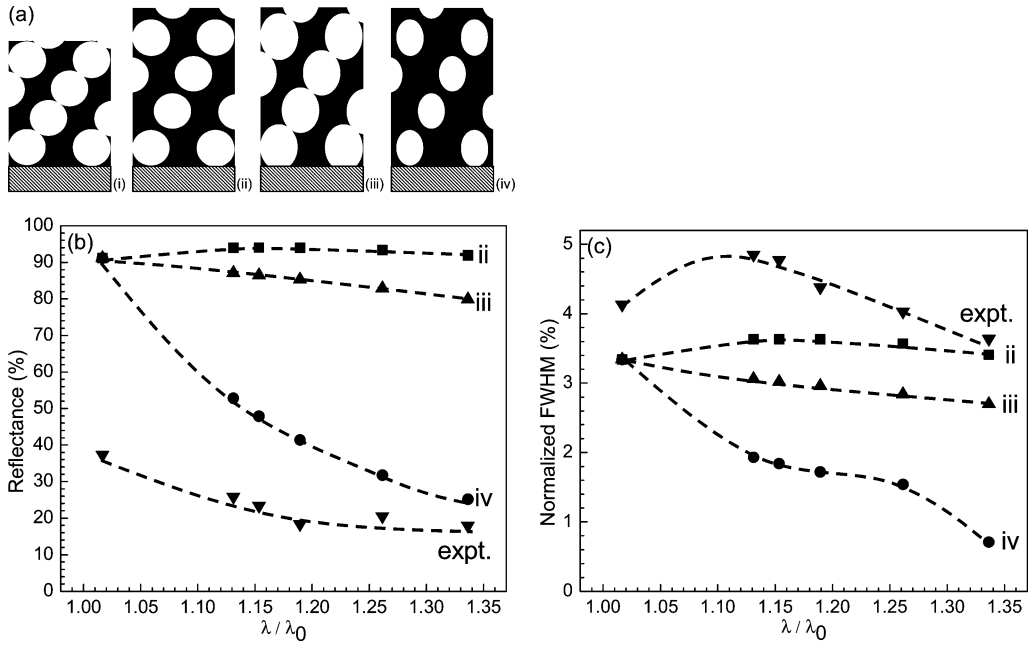

Figure 6. Comparison of experimental and calculated diffraction spectra of hydrogel swelling. (a) Schematic of the hydrogel swelling models: (i) fcc(110) cross section of the fully contracted inverse opal hydrogel on the substrate; (ii) 0-D pore swelling, with no change in pore volume or shape; (iii) 1-D pore swelling, with pores expanding in the same fashion as the bulk hydrogel; (iv) 2-D pore shrinkage, with pores contracting in the substrate normal directions. The overall swelling was assumed to be 1-D due to substrate pinning. (b) Diffraction intensity of 6.25% APBA hydrogel as a function of the total diffraction shift λ/λ_0: inverted triangles, experimental data; squares, 0-D pore swelling; triangles, 1-D pore swelling; circles, 2-D pore shrinkage. Dashed lines are guides for the eye. (c) Normalized fwhm of 6.25% APBA hydrogel as a function of λ/λ_0. The legend is the same as that for panel b.

layers of pores was used for TMM, while 24- and 48-layer inverse opals were used for SWA (the experimentally determined thickness corresponded to ~53 layers). The diffracted peak intensity and normalized fwhm values calculated from the three models using SWA are displayed in Figure 6b,c; the TMM data are qualitatively similar for the 0-D pore swelling case and are not shown (TMM simulations were not done for the 1-D pore swelling and 2-D pore shrinkage cases). Two observations can be made after comparing the calculated and experimental diffraction intensity values (Figure 6b). First, depending on the swelling model used, the diffraction intensity may display drastically different trends. For example, for the 0-D pore swelling case (squares), the diffraction intensity increases slightly with swelling, while diffraction intensity decreased as the hydrogel swelled when using either the 1-D pore swelling (triangles) or the 2-D pore shrinkage model (circles). Second, the simulated diffraction intensity for all three models is much higher than the experimentally observed intensity (inverted triangles), suggesting that factors other than refractive index contrast and pore swelling influence the diffraction intensity of the inverse opal hydrogel. The same variability can be seen in the normalized fwhm data (Figure 6b). While both the 0-D pore swelling model (squares) and the 1-D pore swelling model (triangles) showed a relatively constant fwhm during swelling, the normalized fwhm for the 2-D pore shrinkage model (circles) decreased at high degrees of swelling, comparable to the experimental result (inverted triangles). Thus, to fully understand the evolution of the diffraction peak of the inverse opal hydrogel during swelling, it may be beneficial to directly observe the change in the 3-D pore structure, perhaps through optical microscopy. In addition, a more sophisticated model, such as finite element analysis of hydrogel swelling, may be beneficial.

Discussion

Origin of Glucose Sensitivity at High Ionic Strength. The chemical mechanism for glucose sensing for our inverse opal APBA-functionalized hydrogel is essentially the same as for phenylboronic acid containing PCCA hydrogel glucose sensors.[34] Specifically, formation of a charged complex between phenylboronic acid and glucose increases the degree of ionization on the hydrogel network, causing an influx of solvent and counterions that swell the hydrogel, resulting in a red shift in optical diffraction. However, the hydrogel mesostructures of these two systems are quite different from each other. In our case, infiltration of the dried colloidal crystal with HEMA−APBA mixtures followed by polymerization and template removal resulted in a dense functionalized mesostructure, whereas the PCCA utilized polymerization of a relatively dilute polyacrylamide hydrogel inside a charge-stabilized colloidal crystal which was then functionalized with phenylboronic acid moieties. We believe that the persistence of glucose sensitivity for the inverse opal hydrogel at high ionic strength (Figure 2b and Figure 3) is a direct result of the dense hydrogel structure, which can carry a high concentration of APBA groups. For example, the 6.25% APBA content contained an estimated phenylboronic acid concentration of 515 mM. In comparison, a complete conversion of acrylamide groups in the PCCA into phenylboronic acid moieties would yield a concentration of 14 mM. Thus, even when the anionic APBA−glucose complex is electrically screened at high ionic strength, the larger concentration of ionizable groups in the inverse opal hydrogel allows the mesostructure to swell sufficiently to generate an optical response. The glucose sensitivity of the inverse opal hydrogel at pH 9.5 (Table 1) may also be explained by the higher concentration of APBA groups. Even though a large fraction of the APBA groups are deprotonated at pH 9.5, there is still enough protonated APBA so that complex formation with glucose leads to a significant increase in the equilibrium degree of ionization on the hydrogel. Here, the high solution ionic strength assists in the detection by preventing the hydrogel from becoming fully swollen at pH 9.5, so that the glucose binding could cause a further red shift of diffraction. Based on the glucose sensing data and our previous pH sensing results,[41] we propose that the dense inverse opal hydrogel structure may be especially well suited for detection of analytes at high ionic strength using spectroscopic methods.

Dimensionality of Swelling. Previously, work on a variety of unpinned PCCA hydrogels found that their swelling was 3-D as expected; that is, the dimensionless change in volume $\Delta V/V_0$ was found to be proportional to $(\Delta\lambda/\lambda_0)^3$. Since $\Delta V/V_0$ should be directly proportional to the concentration of ionizable groups on the hydrogel at low degrees of ionization, we compared the calculated $(\lambda/\lambda_0)_b$ values for the 6.25% APBA and the 1.25% APBA hydrogel. We found that the diffraction from the 6.25% APBA hydrogel shifted about 7 times more than that of the 1.25% APBA hydrogel at the same glucose concentration; in other words, a 5-fold increase in ionizable groups led to a 7-fold increase in optical response. This result implies that the charged inverse opal hydrogel does not swell in 3-D but rather mostly in the sample normal direction, which is similar to the behavior of our pH-sensitive hydrogels.[41] This is almost certainly because the hydrogel was covalently attached to the glass substrate and thus could not macroscopically swell in 3-D without delaminating from the substrate; delamination was not observed.

Origin of Diffraction Kinetics and Hysteresis. As mentioned in the results section, the diffraction response of the APBA-functionalized hydrogel follows a $t^{1/2}$ relationship over most of the swelling range, suggesting a diffusion-limited kinetic response. Since pH remained constant while glucose was introduced to the hydrogel, the concentration of H^+ should not impact kinetics. Thus, the diffusion of glucose to reactive APBA sites on the hydrogel is the most likely rate-limiting factor during most of the swelling. The decrease in equilibration time as the hydrogel became more swollen is explained by the effect of expansion on the diffusivity of the hydrogel. The diffusivity of a hydrogel to molecules may be increased by orders of magnitude between the fully collapsed state and the highly swollen state.[60] The generally accepted explanation for this phenomenon is that small molecules generally diffuse through the solvent, and a highly swollen hydrogel mesh contains a higher solvent volume fraction, thereby facilitating molecule diffusion.[61] Thus, as the hydrogel binds to glucose and becomes more swollen, the diffusivity of glucose will increase, and the equilibration time will decrease. The general slowing of the kinetics toward the end of each run may be due to the slow rate of reaction between glucose and the sterically inaccessible APBA functional groups which are buried in the hydrogel structure. When the hydrogel becomes sufficiently swollen, these APBA groups may rotate or translate into configurations where they can bind glucose, leading to a further red shift in diffraction. The dependence of diffusivity on

(60) Gehrke, S. H. *Adv. Polym. Sci.* **1993**, *110*, 81−144.
(61) Yasuda, H.; Peterlin, A.; Colton, C. K.; Smith, K. A.; Merrill, E. W. *Makromol. Chem.* **1969**, *126*, 177.

the swelling ratio may also explain the relatively greater equilibration time and the larger regime of slow diffraction shift kinetics when glucose concentration was decreased. Since the glucose diffuses out of the top of the hydrogel film into the bulk solution first, this is the first region to contract, and since the contracted state has a lower diffusivity for glucose it could retard further outflow. The kinetically trapped interior regions reach equilibrium more slowly, explaining the apparent hysteresis in diffraction response observed over the time frame of our experiment (~30 min) which disappeared overnight.

Comparison of Experimental and Theoretical Diffraction Spectra. As mentioned, a comparison of the experimental diffraction spectra versus the peak parameters simulated using SWA revealed a large discrepancy in diffraction intensity (Figure 6b) and normalized fwhm (Figure 6c). Since the hydrogel swelling is accompanied by an influx of water and counterions, the refractive index contrast between the hydrogel phase and the aqueous solution should decrease with swelling, which should in turn decrease the normalized fwhm of the diffraction peak for the swollen hydrogel. However, the change in the shape of the pores should also be considered. Our 0-D pore swelling model accounted for the decreasing refractive index contrast but not changes in pore dimensions. In this model, both calculated diffraction intensity and normalized fwhm increased and then decreased slightly as the diffraction shift increased (squares), whereas the experimental diffraction intensity (inverted triangles) decreased significantly as the hydrogel swelled. Thus, variation in refractive index contrast alone was insufficient to predict the shape of a diffraction spectrum as a function of hydrogel swelling. The 1-D pore swelling model yielded diffraction spectra that are slightly more similar to the experimental data but still qualitatively different. Over the entire range of hydrogel swelling, the calculated diffraction intensity and normalized fwhm each decreased by ~10% versus their initial values (triangles). The 2-D pore shrinkage model, which is most physical in that it allows the hydrogel to expand into all available volumes, is qualitatively closest to the experimental data. For this model, the diffraction intensity decreased monotonically, with an intensity $\sim^1/_3$ of its starting value at a diffraction shift of 1.34 (Figure 6b, circles), which was similar to the experimental diffraction intensity decrease of $\sim^1/_2$ (Figure 6b, inverted triangles). Thus, the experimental trend in peak intensity can be partially explained by a combination of decreasing refractive index contrast and partial pore closure.

There are several variables not accounted for with our models and simulation methods. One factor is disorder of the inverse opal hydrogel due to drying cracks and crystal defects of the colloidal template. The presence of such disorder is clear, as shown by the reflection optical micrographs (Figure 1b,c) and SEM (Figure 1e). In addition, the well-defined Fabry−Perot interference fringes disappeared as the hydrogel swelled (Figure 2a), suggesting the flat interfaces at the top and bottom of the hydrogel were disrupted, possibly due to inhomogeneous swelling. The disorder initially present in the templated hydrogel should result in lower diffraction intensity and higher fwhm due to interruption of the 3-D translational order. Since these defect sites are filled with hydrogel, they tend to swell more drastically as the rest of the hydrogel expands, which may cause the templated hydrogel to become increasingly disordered during swelling. The contributions of disorder may help explain the much lower initial diffraction intensity of the hydrogel film compared with its theoretical predictions (Figure 6b), as well as the higher than predicted values for normalized fwhm (Figure 6c). In addition, the higher swelling in the defect sites may create local stress points that can buckle the surrounding structure, resulting in a large scatter in the normalized fwhm values (Figure 5).

Our microspectroscopy on the dried poly(styrene)−air colloidal crystal used as the template found the diffraction intensity was on the order of ~60%, when theory predicted that nearly 100% of the light should be reflected, given the high refractive index contrast between poly(styrene) and air. Thus, improving the order of the colloidal template is important in optimizing the diffraction response of an inverse opal hydrogel sensor. Nevertheless, since our sensing mechanism depends on the change in diffraction wavelength rather than intensity, the current diffraction efficiency is probably sufficient for most sensing applications. Changes in the 3-D mesostructure must also be considered as a factor affecting the resulting reflection spectra. We are currently studying the evolution of pore shape as a function of swelling both experimentally and through finite element techniques and hope to couple this with optical simulations and experimentally obtained spectra.

Error Analysis. In Figure 4 and Figure 5, curve fitting was performed on the experimental diffraction spectra to quantitatively study kinetics and equilibrium peak shapes, respectively. The error bars for diffraction wavelength, peak intensity, and normalized fwhm generated by the least-squares peak fit were very small and thus were not plotted. For example, the averages for the normalized error (error divided by the data value) for diffraction wavelength, diffraction intensity, and normalized fwhm in Figure 4a,b were 6.2×10^{-5}, 6×10^{-3}, and 6×10^{-3}, respectively. The average normalized errors for the corresponding parameters in Figure 5 were 4×10^{-5}, 4×10^{-3}, and 3×10^{-3}. It is clear that the peak fitting algorithm is more proficient at fitting the diffraction wavelength than the other two peak parameters, as shown by its significantly smaller error. This may explain why the data points in Figure 4a,b, which plotted the diffraction wavelength, formed a smoother line than the data in Figure 5 dealing with the peak intensity and normalized fwhm. In addition, the diffraction spectra in Figure 4a,b contained higher errors when compared with corresponding values generated from Figure 5. This may be explained because the kinetics data in Figure 4a,b were acquired over a shorter time interval than the steady-state data in Figure 5 (1 s vs 7.5 s), which reduced the signal-to-noise ratio of each spectrum. Finally, the signal resolution of the diffraction spectrum is limited by the diffraction grating spectrophotometer, which contains 512 elements arrayed over the range 290−1100 nm. Thus, all peaks have a minimum uncertainty of 1.6 nm.

Conclusions. Utilizing dried colloidal crystals as templates, we synthesized phenylboronic acid functionalized inverse opal hydrogels within microfluidic flow cells for glucose sensing. The diffraction response was characterized with a maximum diffraction shift due to glucose binding of 1.201 for 6.25% APBA hydrogel at 100 mM glucose. The dependence of swelling on the concentration of the APBA functional group and the lack of delamination from the substrate suggested that the templated hydrogel preferentially swelled in the substrate normal direction. Detectable diffraction response was observed for ionic strengths as high as 326 mM; the ability to sense glucose at physiological and higher ionic strengths may be attributed to a higher concentration of APBA groups in a dense hydrogel than is achievable by previous PCCA techniques. Diffraction response kinetics followed a $t^{1/2}$

relationship, with an equilibration time of ~1100 s for physiological ionic strength and glucose concentrations, suggesting slow, diffusion-limited kinetics. At equilibrium, the diffraction peak intensity decreased monotonically with swelling, with a maximum intensity reduction of $\sim^1/_2$ at a diffraction shift of 1.34, while the normalized fwhm remained at ~4−5%. Comparison to simulated reflection spectra suggests that the trend in diffraction intensity as a function of swelling can be partially explained by a combination of the decrease in refractive index contrast and an appropriate pore deformation model. In addition, sample disorder and/or changes in the 3-D mesostructure due to pore deformation may contribute to the discrepancy between simulated and experimental values of diffraction intensity and normalized fwhm.

Acknowledgment. This material is based in part upon work supported by the U.S. Department of Energy, Division of Materials Sciences, under Award No. DEFG02-91ER45439, through the Frederick Seitz Materials Research Laboratory at the University of Illinois at Urbana-Champaign and through the DOE S&P Center program. Research for this publication was carried out in the Center for Microanalysis of Materials, University of Illinois at Urbana-Champaign, which is partially supported by the U.S. Department of Energy under Grant DEFG02-91-ER45439, and in the Imaging Technology Group at the Beckman Institute, UIUC. We thank Dr. Hiromi Kitano (Toyama University, Toyama, Japan) for the detailed recipe for synthesizing 3-acrylamidophenylboronic acid, M. Meitl (UIUC) for assistance with SEM imaging, and fellow group members S. Mariserla for performing APBA synthesis and H. Tu for NMR characterization.

Supporting Information Available: Development of the pore-deformation models to be inputted into the SWA calculations and additional experimental data from an oxygen plasma treated APBA hydrogel. This material is available free of charge via the Internet at http://pubs.acs.org.

LA035555X